Applied Surface Science 441 (2018) 372–380

Contents lists available at ScienceDirect

Applied Surface Science

journal homepage: www.elsevier.com/locate/apsusc

Full Length Article

Femtosecond laser irradiation on Nd:YAG crystal: Surface ablation and high-spatial-frequency nanograting

Yingying Ren [a,b,*], Limu Zhang [a], Carolina Romero [d], Javier R. Vázquez de Aldana [d], Feng Chen [c,*]

[a] Shandong Provincial Key Laboratory of Optics and Photonic Device, School of Physics and Electronics, Shandong Normal University, Jinan 250014, China
[b] Institute of Data Science and Technology, Shandong Normal University, Jinan 250014, China
[c] School of Physics, State Key Laboratory of Crystal Materials, Shandong University, Jinan 250100, China
[d] Laser Microprocessing Group, Departamento de Física Aplicada, Universidad de Salamanca, Salamanca 37008, Spain

ARTICLE INFO

Article history:
Received 18 September 2017
Revised 25 January 2018
Accepted 25 January 2018
Available online 20 February 2018

Keywords:
Femtosecond laser irradiation
Laser-induced micro-structures
Nanogratings
Nd:YAG crystal

ABSTRACT

In this work, we systematically study the surface modifications of femtosecond (fs) laser irradiated Nd:YAG crystal in stationary focusing case (i.e., the beam focused on the target in the steady focusing geometry) or dynamic scanning case (i.e., focused fs-laser beam scanning over the target material). Micro-sized structures (e.g. micro-craters or lines) are experimentally produced in a large scale of parameters in terms of pulse energy as well as (effective) pulse number. Surface ablation of Nd:YAG surface under both processing cases are investigated, involving the morphological evolution, parameter dependence, the ablation threshold fluences and the incubation factors. Meanwhile, under specific irradiation conditions, periodic surface structures with high-spatial-frequency ($<\lambda/2$) can be generated. The obtained period is as short as 157 nm in this work. Investigations on the evolution of nanograting formation and fluence dependence of period are performed. The experimental results obtained under different cases and the comparison between them reveal that incubation effect plays an important role not only in the ablation of Nd:YAG surface but also in the processes of nanograting formation.

1. Introduction

The interaction of ultrafast laser pulses with solids has gained remarkable attraction over the past decades due to the increasing availability of commercial ultrafast laser sources along with the improvement in corresponding physical mechanisms [1–3]. Ultrashort ablation exhibits advantages in terms of high resolution and geometric flexibility of the fabricated structures. Through ultrafast laser irradiation, the local intensity distribution can be engineered via tailoring the irradiation parameters, achieving various kinds of modifications on different materials. Micrometer-sized structures in dielectric materials produced by laser irradiation, such as micro-craters or micro-channels, have been investigated experimentally and theoretically [4–14]. Upon ablation of these materials with laser pulses, usually two cases are performed which are "stationary focusing case" with the beam focused on the target surface in the steady focusing geometry and "scanning case" with focused fs-laser beam scanning over the target material. It has been revealed that, during multiple laser pulse micromachining, the incubation effect, which is related to the laser induced defects, influence the ablation threshold and thereby is partly responsible for the formation of micro-structures [6,11–14]. For both practical and theoretical reasons, it is crucial to determine the laser-induced damage threshold of certain material. Such threshold relies on the material properties together with the laser parameters such as pulse number or scan speed. Several experimental approaches have been established for the determination of the laser ablation threshold of a material [10].

Since the pioneering work by Birnbaum early in 1965 [15], significantly increasing research works have been focused on laser-induced periodic surface structures (LIPSS, so called ripples), among which nano-sized grating structures (i.e., nanogratings) generated by direct femtosecond laser irradiation have been widely reported. By irradiating with the tightly focused laser pulses on the surface or in the bulk of materials, nanogratings could be created in either stationary case or scanning case with the nanoscale arrangement underlying in the central area of the focal spot (for the former case) [8,16–21], in the cross-section of irradiated line [22–25] or in the scanned volume (for the latter case) [13,17,23,26–29]. Up till now, representative dielectric solids utilized for nanograting formation is fused silica [8,13,16–20,24–28] and sapphire [5,6,22,23,29], whilst a relatively small number

* Corresponding authors at: Shandong Provincial Key Laboratory of Optics and Photonic Device, School of Physics and Electronics, Shandong Normal University, Jinan 250014, China (Y. Ren).
E-mail addresses: ryywly@sdnu.edu.cn (Y. Ren), drfchen@sdu.edu.cn (F. Chen).

https://doi.org/10.1016/j.apsusc.2018.01.217
0169-4332/

of research activities are about materials such as TeO_2, LiF, MgF, BaF_2, CaF_2, ZnO [8,16,21,30–32]. Many investigations are conducted to study the origin of nanograting on these materials as a function of irradiation parameters. Apart from the laser wavelength, repetition rate, pulse duration, pulse delay and focusing condition, parameters including laser polarization, laser fluence, pulse number, as well as the scan speed have been proved to be essential for controlling the formation of the nanograting. For LIPSS produced by linearly polarized laser beam in dielectrics, low-spatial-frequency LIPSS (LSFL) with a period close to the irradiation wavelength λ or close to λ/n (where n represents the refractive index of the material) [18] or high-spatial-frequency LIPSS (HSFL) which has spatial periods significantly smaller than λ (under certain condition, equal to λ/2n) [17,19,22–28,30] are usually observed in the ablated area, showing an alignment either perpendicular or parallel to the laser polarization. Additionally, hybrid structures with LSFL surround by HSFL are obtained under either stationary case [20,21,31,32] or scanning case [29]. Additionally, LSFL with a novel annular morphology which is independent of the laser polarization and universally observed for different focusing geometries are demonstrated on fused silica [33]. However, the nature of the formation of LIPSSs is still quite controversially discussed. Incubation effect, which is responsible for the ablation threshold of the materials, has been found to be crucial during the formation of nanograting [13,17,19].

Such micro-sized structures and nano-sized LIPSSs show promising potential in micromachining for the realization of 3D microchannels, nanofluidic devices, optical storage devices, polarization converters and so on. In this work, we systematically explore, for the first time to our knowledge, the evolution and formation of fs-laser induced micro-sized structures and nano-sized LIPSSs on the surface of Nd:YAG crystal in the stationary focusing case as well as in the dynamic scanning case. In this latter case, the fs-laser beam adopted is polarized either parallel or perpendicular to the scan direction. The parameter dependence of laser ablated regions on Nd:YAG surface under various conditions of pulse energies and pulse numbers (or scan speed) are investigated and analyzed by utilizing scanning electron microscopy (SEM). The laser induced ablation threshold fluences and incubation factors of Nd:YAG under two cases are obtained based on the diameter-regression technique and incubation equation. More importantly, LIPSSs are produced in both cases under certain parameters, revealing that high quality LIPSSs could be produced by adjusting incident laser in terms of laser energy as well as pulse number (or scan speed). The periods of LIPSSs are measured, showing the formation of high-spatial-frequency surface nanograting on Nd:YAG crystal. Their dependences on irradiation parameters are also investigated. We evidence that incubation effect plays a pivotal role not only in the process of Nd:YAG ablation and but also in the generation of nanogratings on Nd:YAG surface.

2. Experiments in details

The Nd:YAG crystal selected for this work is doped by 1 at.% Nd^{3+} ions and optically polished. Several exposures are performed on the sample surface by employing fs-laser either in the stationary focusing case or in the dynamic scanning case with different parameters including pulse energy, number of shots, scan speed and laser polarization. A commercial 120-fs Ti:Sapphire regenerative amplifier (Spitfire, Spectra Physics, USA) is used as fs-laser source to deliver linearly-polarized pulses at central wavelength of 795 nm with 1 kHz repetition rate. The laser polarization and the incident energy are adjusted with a half-wave plate and a linear polarizer placed before a calibrated neutral density filter. After being focused by a 10× microscope objective, the laser beam is irradiated on the target which is mounted on a computer controlled XYZ motion stage. After irradiation, in order to remove the debris from the laser modified regions for analyzing, ablated sample is etched in 50% phosphoric acid for 5 min and subsequently cleaned in an ultrasonic bath. Afterwards, the sample surface is analyzed by scanning electron microscopy.

In the stationary focusing case, the number of incident pulses reaching each spot of the sample is controlled with a mechanical shutter (Uniblitz). Fig. 1(a) shows the schematic of the laser irradiation procedure in this case. A series of ablation spots are created in the surface with different pulse energies from 0.2 μJ to 8.0 μJ and the number of shots ranging from 5 to 10,000 per site. As shown in Fig. 1(b), which is the optical microscope image of modified surface obtained on Nd:YAG surface in stationary case, the ablation can be observed for all of the irradiating conditions. In the dynamic scanning case, two different approaches are tested with the electric field of the fs-laser E either parallel or perpendicular to the scanning direction S, as illustrated schematically in Fig. 1(c). The pulse energies used for both approaches are changed from 0.032 μJ up to 4.0 μJ and the scan speeds are varied from 5 μm/s to 200 μm/s. Fig. 1(d) shows the optical microscope images of the irradiated lines on Nd:YAG surface. It is found that when pulse energy is lower than 0.11 μJ, the irradiated areas are very difficult to be observed.

3. Results and discussion

3.1. Micro-structures produced in stationary focusing case

In the stationary focusing case, four regimes of isolated modifications are induced by different pulse numbers and energies, which can be located within a process window visualizing the different types of modifications and corresponding process parameters (REGIME I-IV in Fig. 2(a)). The SEM micrographs in Fig. 2(b)–(e) compare some femtosecond pulse laser-induced modifications in REGIME I and IV for different parameters of: (b) 0.2 μJ, 5 shots; (c) 0.6 μJ, 20 shots; (d) 8 μJ, 200 shots; (e) 8 μJ, 1000 shots. In REGIME I, superficial and smooth modification is observed as shown in Fig. 2(b)–(d). In contrast with REGIME I, well-shaped LIPSSs are fabricated in REGIME III. Between REGIME I and III, a transitional modification pattern (denoted RANGE II) is detected. Both of the REGIME II and III will be discussed in detail later. In RANGE IV, ultra-deep craters are induced by high pulse energy and massive pulse number, as shown in Fig. 2(e).

Regardless of the emergence of LIPSSs, the damage size D induced by fs-laser depends on the fluence used with respect to the laser-induced ablation threshold (LIAT) of the material, which, in turn, can be determined by measuring the diameter of the ablated areas. The relation between them can be given by:

$$D^2 = 2\omega^2 \ln\left(E_p/E_{th}\right) \quad (1)$$

where E_p is the experimentally measured pulse energy, E_{th} is the LIAT energy and ω is the effective radius of Gaussian beam. In Fig. 3(a), squared diameters D^2 are plotted as a function of the laser pulse energy $\ln(E_p)$ for 5 pulse processing. By extrapolating the linear fit (blue line) to D^2=0, the effective beam radius and surface LIAT energy can be determined (so called the diameter-regression technique [10]). With 5 pulse irradiation, the effective radius ω = 1.7 μm of the laser spot is calculated and the LIAT energy E_{th} is computed to be 0.20 μJ, corresponding to a LIAT fluence F_{th} of 4.38 J/cm^2. In this work, the lowest laser energy utilized at 5 pulses is near the threshold value, therefore yielding a superficial modification. Similar calculations for values of pulse number up to 10,000 enable to determine the effective beam radii and LIAT fluences at different pulse numbers. It can be seen from Fig. 3(b) that the effective radius

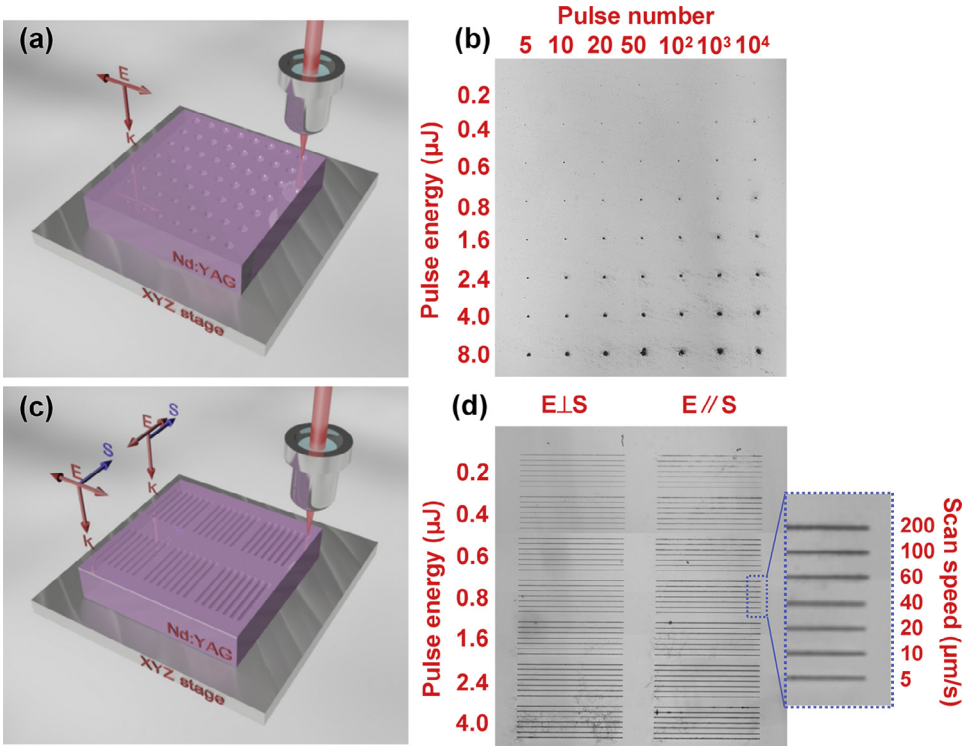

Fig. 1. Schematic of fs-laser irradiation process and optical microscope observation of the writing areas on Nd:YAG surface in stationary focusing case ((a) and (b)) and dynamic scanning case ((c) and (d)). The machining parameters are included in (b) and (d). K: Laser propagation direction; E: Electric field; S: Scan direction.

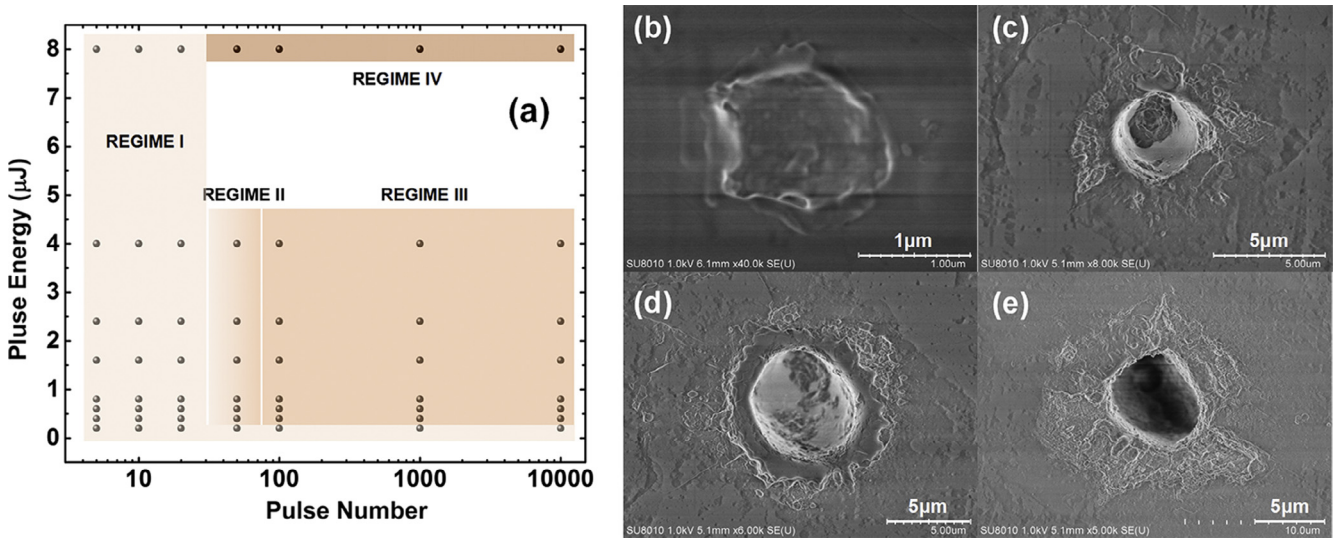

Fig. 2. (a) Process window of irradiation in stationary focusing case with localization of different types of modifications corresponding to REGIME I-IV. (b)–(e) Some SEM images of Nd:YAG crystal surface after irradiation with laser pulses of different parameters.

of the laser beam increases with the pulse number, revealing the decrease of LIAT fluence, which is induced by multipulse related incubation effect. However, the effective beam radii reach a saturation at around 1000 pulses, indicating the saturation of the incubation effect. The red balls in Fig. 3(c) display the calculated LIAT fluences as a function of pulse numbers. As expected, the LIAT fluence of Nd:YAG crystal decreases dramatically for small pulse number and then becomes saturated at the pulse number of about 1000.

In stationary focusing case, the incubation effect could be described by equation:

$$F_{th}(N) = F_{th}(\infty) + [F_{th}(1) - F_{th}(\infty)]\exp[-k(N-1)] \quad (2)$$

where $F_{th}(\infty)$ is the threshold fluence at an infinite numbers of pulses, $F_{th}(1)$ is the single pulse ablation threshold and k is an empirical parameter (so called incubation factor). According to the incubation equation Eq. (2), the experimental data of threshold fluence at different pulse numbers can be fit exponentially with a single pulse ablation threshold of 4.46 J/cm^2, an infinite pulse ablation threshold of 2.46 J/cm^2 and an incubation factor k of 0.005, as shown with black line in Fig. 3(c). Therefore, compared with the single pulse ablation $F_{th}(1)$, the threshold reduced approximately 45% when it reaches saturation value.

Additionally, the crater diameters can be plotted as a function of pulse fluences for different pulse numbers as depicted in Fig. 3(d).

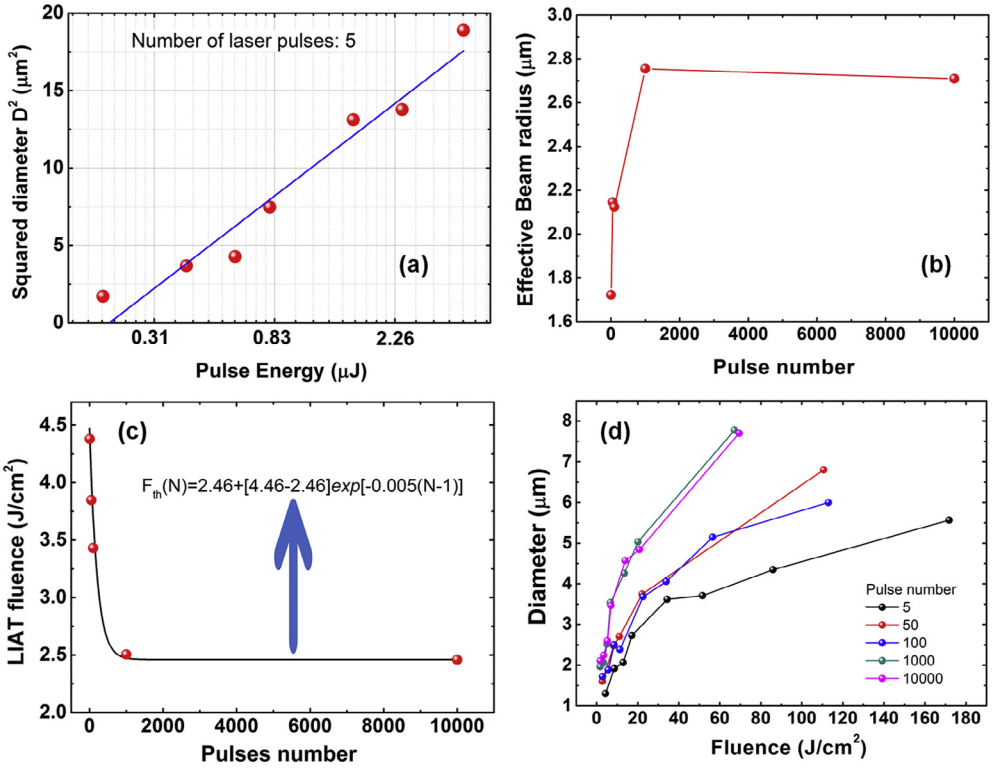

Fig. 3. (a) Squared diameter D^2 of the ablated area as a function of the pulse energy $\ln(E_p)$ for 5 pulse processing. (b) Calculated effective beam radius versus the pulse number. (c) LIAT fluence versus laser pulse number for Nd:YAG crystal in stationary focusing case. Ball symbols represent experimental data; solid line represents the fitting result from following Eq. (2). (d) Fluence dependence of the diameters of the ablated areas on Nd:YAG surface. The lines guide the eye.

As can be seen clearly that with increasing pulse fluences under fixed pulse number, the diameters of irradiated craters increase monotonously, following a semi-logarithmic representation.

3.2. Micro-structures produced in dynamic scanning case

In analogy to the study of static irradiation, the structures fabricated in the scanning case are investigated with SEM. Based on the SEM graphs of the modified structures, neglecting the formation of LIPSSs, the structural overall widths are investigated. In consequence, the ablation threshold of micro-sized scanned line can be calculated with the diameter-regression technique by simply replacing damaged diameter with structural width in Eq. (1). In this situation, the ablation threshold fluences F_{th} for scan speed of, for instance, 5 μm/s are determined to be around 1.83 J/cm^2 (E_{th} = 0.18 μJ, ω = 2.5 μm) and 2.4 J/cm^2 (E_{th} = 0.19 μJ, ω = 2.3 μm) corresponding to the approaches with E parallel to S and E perpendicular to S respectively.

During the scanning process, different scan speeds result in different numbers of pulses irradiating the sample. The effective pulse number N_{eff} that impinges on each point can be determined as:

$$N_{eff} = \omega/d = \omega f/v \quad (3)$$

in which d is the pulse-to-pulse space, f is the repetition rate of the laser pulses (1 kHz in this work) and v equals to the scan speed. Consequently, the surface LIAT fluence under scanning case as a function of the effective pulse number can be obtained as shown in Fig. 4(a) and (b). The incubation equation for scanning irradiation is considered to be the same with Eq. (2) in which N represents effective pulse number N_{eff}, and thus the calculated data of LIAT fluences can be fit accordingly (see exponential curves in Fig. 4(a) and (b)). The incubation equation for the situation of E parallel to S is determined to be F_{Neff} = 1.82 + 0.62 × exp[-0.01×(N_{eff} − 1)], deriving a single shot LIAT fluence of 2.44 J/cm^2 together with an infinity pulse LIAT fluence of 1.82 J/cm^2. As for the case of E perpendicular to S, the obtained single and infinity shot LIAT fluence are 3.1 J/cm^2 and 2.37 J/cm^2 respectively and the incubation equation can be described as F_{Neff} = 2.37 + 0.73 × exp[−0.009 × (N_{eff} − 1)]. The factor k that characterizes the strength of incubation for two approaches are thus estimated to be 0.01 and 0.009 which are higher than that obtained from stationary case (k = 0.005). It is therefore reasonable to conclude that the incubation is influenced not only by the number of pulses that impinged on the sample surface but also on the laser-irradiating approaches. The incubation factor obtained in our work for Nd:YAG crystal is much smaller than the previously reported values for, such as, sapphire crystals [6,29], lithium niobate crystal [14] and glass [11,13]. Nonetheless, it would be expected though, that the incubation factor is low but very important for the ablation of Nd:YAG crystal.

Moreover, the development of structural overall width as a function of pulse fluence is investigated, as documented in Fig. 4 (c) and (d) for two different approaches (E//S and E⊥S), which obviously show very similar variation trends. For fixed scan speed (i.e., fixed effective pulse number), the widths of the structures increase with pulse fluences. Additionally, similar to the stationary focusing case, a scanning laser beam results in a damage whose width scales with a semi-logarithmic law which, in turn, indicates the identical behavior of laser fluence deposition into the Nd:YAG crystal during static and dynamic ablation process.

3.3. Nanogratings produced in stationary focusing case

In the stationary focusing case, periodic ripples are produced in the laser ablated craters with processing laser energies from 0.4 μJ to 4 μJ and pulse number equal to or greater than 100. With a lower number of laser pulse of 50, only small grooves are initiated

without clear indications of LIPSSs when pulse energy is higher than 0.2 μJ, which can be considered as transition states between smooth modification and LIPSSs. In Fig. 5, two transitions are shown corresponding to 50 laser shots at pulse energies of 0.6 μJ (Fig. 5(a)) and 0.8 μJ (Fig. 5(b)), respectively. Shallow grooves can be recognized at the bottom of the crater, as indicated by red

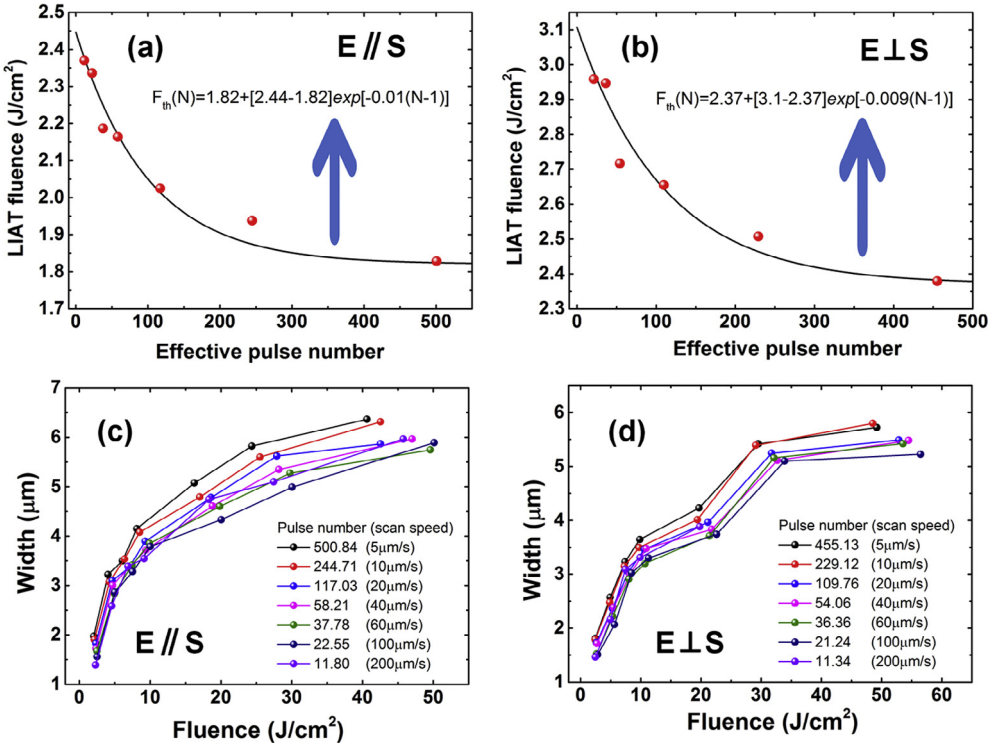

Fig. 4. LIAT fluence versus effective laser pulse numbers for Nd:YAG crystal in dynamic scanning case for approaches with laser polarization parallel (a) or perpendicular (b) to the scanning direction. Balls represent experimental data; solid lines represent the fitting results. Fluence dependence of the widths of the ablated lines on Nd:YAG surface with laser polarization parallel (c) or perpendicular (d) to the scanning direction. The lines guide the eye.

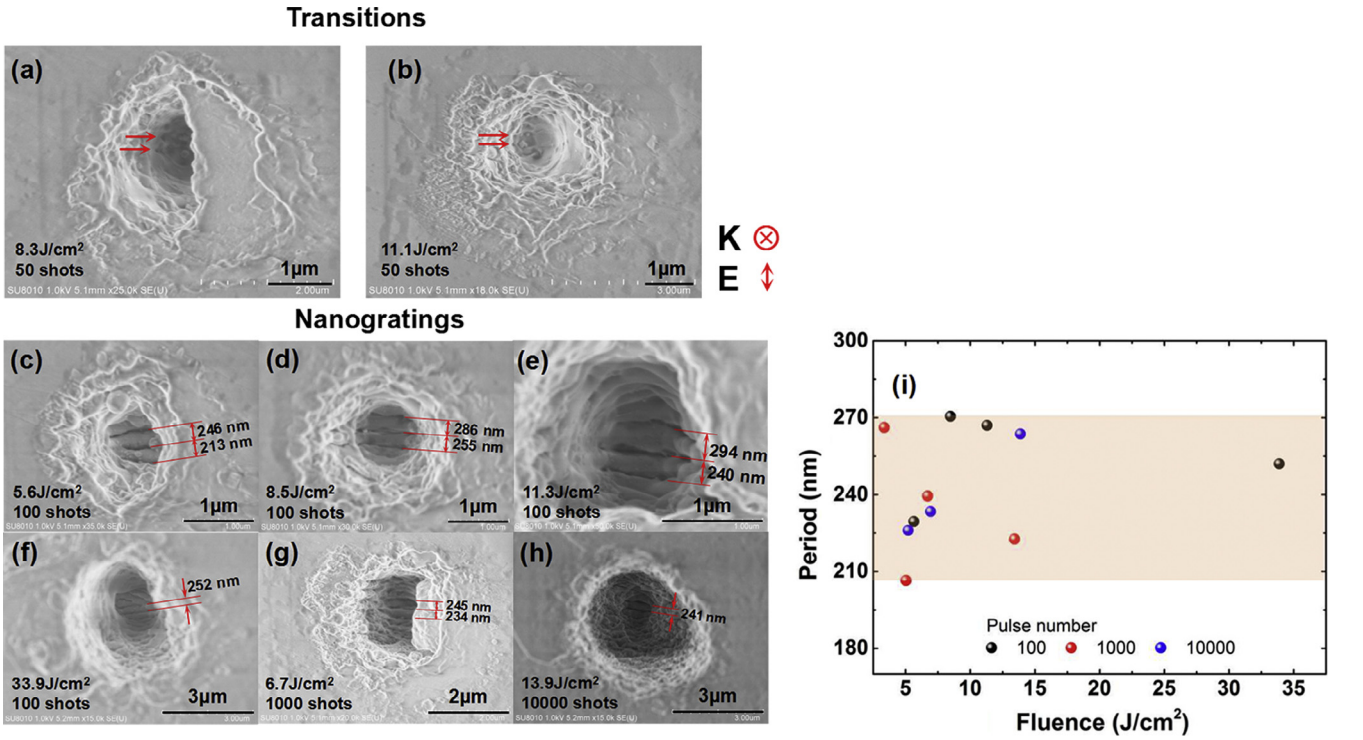

Fig. 5. Nanogratings formed on Nd:YAG surface in stationary focusing case. (a) and (b) Transition states between smooth modifications and LIPSSs, (c)–(e) Well-organized nanograting structures correspond to pulse number of 100 and pulse energies ranging from 0.4 μJ to 0.8 μJ. (f)–(h) Three examples of slightly disordered nanogratings with either pulse energy or pulse number well above the critical value. (i) Nanograting periods produced with different parameters in stationary focusing case.

arrows. Consequently, with static irradiation, the critical number of pulses for nanograting generation in Nd:YAG crystal can be estimated to be around 50. Furthermore, as previously mentioned, at the lowest laser energy of 0.2 μJ, the material only suffers a moderate modification without the appearance of grooves. When the laser energy increases slightly to 0.4 μJ, a pronounced change happens and obvious ripples appear at the bottom of the laser-irradiated craters, as shown in Fig. 5(c) for instance. Obviously, at a fixed number of laser pulses larger than 50, there is a critical fluence threshold for the formation of LIPSSs, above which a transition from smooth modification to LIPSSs occurs. This threshold for ripple formation on Nd:YAG crystal under our experimental conditions is slightly higher than the laser-induced ablation threshold, corresponding to pulse energy larger than 0.2 μJ but lower than 0.4 μJ. According to our experimental observation, the best three LIPSSs that feature distinct, uniform and parallel grooves are obtained when the pulse number is 100 and pulse energies range from 0.4 μJ to 0.8 μJ, as shown in Fig. 5(c)–(e). When the pulse energy or pulse number is well above the critical value, deep and rough craters are formed accompanied by slightly disordered ripples, as shown in Fig. 5(f)–(h). Therefore, in order to fabricate LIPSSs of high quality with a stationary focused laser beam on Nd:YAG surface, the incident laser should be adjusted in terms of laser energy as well as pulse number.

For a quantitative analysis of the LIPSS periods, the average spacing of grooves at the bottom of each crater is measured (as shown in Fig. 5(c)–(h)) and plotted in Fig. 5(i). It can be seen that the periods are between 206.5 nm and 270.5 nm (0.25λ–0.34λ), indicating the formation of high-spatial-frequency LIPSSs (i.e., nanogratings). The orientations of the created nanogratings are perpendicular to the laser beam polarization.

3.4. Nanogratings produced in dynamic scanning case

3.4.1. Irradiation with the laser beam polarized along the scan direction

Under this irradiating condition, the evolution of nanograting formation experiences progressive stages involving the generation of nano-craters, the connection of nano-craters, the development of intermittent nanogratings and, finally, the formation of periodic nanogratings, which can be evidenced by the SEM images of irradiated regions with pulse energy of 0.4 μJ and scan speed ranging from 200 μm/s to 40 μm/s as shown in Fig. 6(a)–(d). At the scan speed of 200 μm/s, which corresponds to an effective pulse number of 12, isolated nano-craters are formed and distributed randomly on the irradiated areas as can be seen from Fig. 6(a). Nano-grooves are initially shaped at around 22 shots as shown in Fig. 6(b). With a further increasing number of incident pulses, as seen from Fig. 6(c), periodic structures emerge in certain fragment of the scan line, which are transitions between smooth modification and LIPSS morphologies. When the pulse number is increased to 58 (corresponding to a scan speed of 40 μm/s), well-shaped nanograting structures are formed as shown in Fig. 6(d).

By using this scanning approach, LIPSSs are produced with pulse energy from 0.2 μJ to 4 μJ when the scanning speed is systematically varied from 5 μm/s up to 60 μm/s, corresponding to an effective number of pulse of 500.84 to 37.78 at each point of the sample. Fig. 6(e)–(m) show some SEM images of the irradiated surface. Owing to the Gaussian shape of the laser beam profile, the ripples are located in the center of the irradiated lines. Additionally, long-range order is evident and the ripple direction is perpendicular to the direction of laser polarization. At the lowest pulse energy of 0.2 μJ and lowest scan speed of 5 μm/s, which corre-

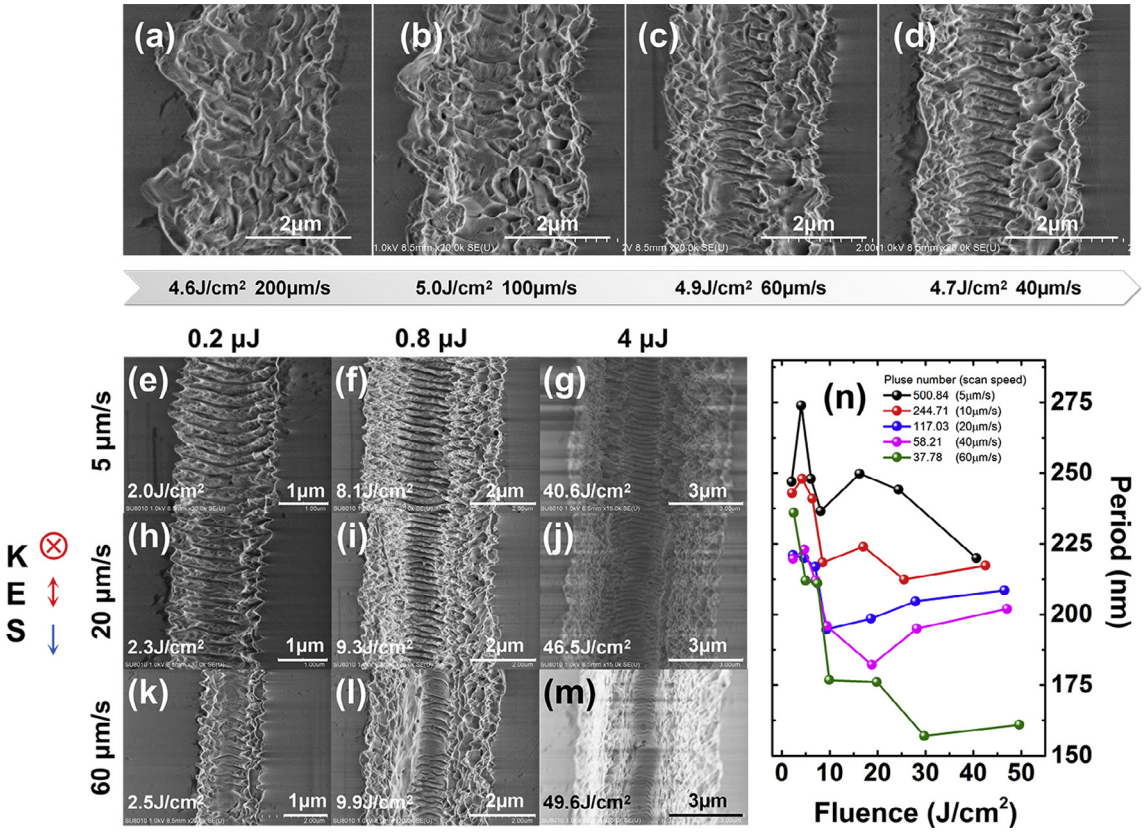

Fig. 6. Evolution of nanogratings formed with pulse energy of 0.4 μJ on the surface of Nd:YAG in scanning case with laser polarization parallel to the scanning direction. (a) Generation of nano-craters; (b) Connection of nano-craters; (c) Development of intermittent nanogratings; (d) Formation of periodic nanogratings. (e)–(m) Nanogratings formed on the surface of Nd:YAG crystal in scanning case with laser polarization parallel to the scan direction. (n) Nanograting periods as a function of pulse fluences. The lines guide the eye.

spond to a pulse fluence of 2.0 J/cm^2 and an effective pulse number of 500.84, very well-organized ripples that occupy the entire scan line transversely are observed at the sample surface.

Quantitative evaluation of the LIPSS period is also performed by measuring the mean distance between two adjacent grooves. The periods of the transitions are measured by selecting regions with continuous ripples. It is found that high-spatial-frequency nanogratings are also obtained with periods between 274 nm and 157 nm (0.20λ–0.34λ). Fig. 6(n) shows the corresponding results of period measurement in terms of pulse fluence dependence. One notes that at fixed scan speed, in general, the period of LIPSSs decreases with the increase of pulse fluence. Such a fluence dependence of period is coincident with that obtained from nanograting structures on fused silica [27].

3.4.2. Irradiation with the laser beam polarized perpendicular to the scan direction

Upon fs-laser pulse irradiation of Nd:YAG with E perpendicular to S, ripple morphologies are observed under the irradiation conditions with pulse energy from 0.2 μJ to 4 μJ and scanning speed lower than 60 μm/s. SEM micrographs in Fig. 7(a)–(d) show the LIPSSs generated on the bottom of the irradiated regions with different parameters. As shown in Fig. 7(a), by irradiating with the lowest pulse energy and translation speed, two parallel grooves are induced, which are aligned along the scan direction (i.e., perpendicular to the writing laser polarization). At higher pulse energy and scan speed, an interesting phenomenon shows up. As can be seen in Fig. 7(b)–(d), the induced grooves tilt almost symmetrically from the central axis of the stripe region towards two sides of the scan line. Despite this tilt, the grooves on the same side of the central axis are parallel to each other and profiled equidistantly. Consequently, the average distances between adjacent parallel grooves, as indicated with red lines in Fig. 7(d), are measured, which is considered to be the period (Λ) of the ripple structures. The results of measurement are plotted in Fig. 7(e), which indicates the fluence dependence of LIPSSs. Identically, the period Λ, which varies from 203.4 nm to 344.3 nm (corresponding to 0.25λ–0.43λ), is decreased with the increment of the pulse fluence. Moreover, by carefully investigating the profile of the ripples and the location of each groove, it is not difficult to identify that, besides the main period Λ, a second period Λ_s that are parallel to the direction of translation is yielded by fs-laser scanning. The yellow arrows in Fig. 7 (b)–(d) point the tips of some grooves, which are the onset (or offset) of the corresponding cycles. Hence, the period Λ_s can be deter-

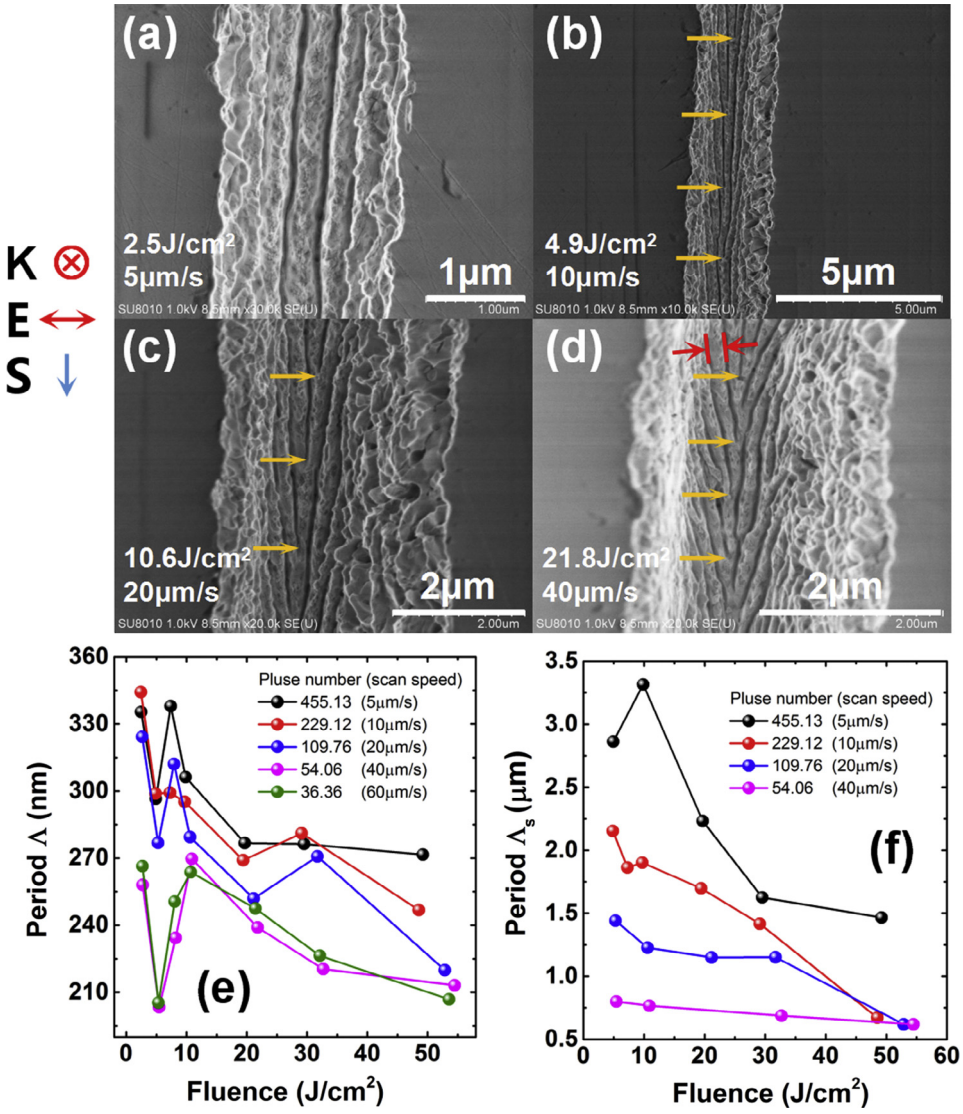

Fig. 7. (a)–(d) Nanogratings formed on the Nd:YAG surface in scanning case with laser polarization perpendicular to the scan direction. Nanograting periods Λ (e) and second periods Λ_S (f) as a function of pulse fluences. The lines guide the eye.

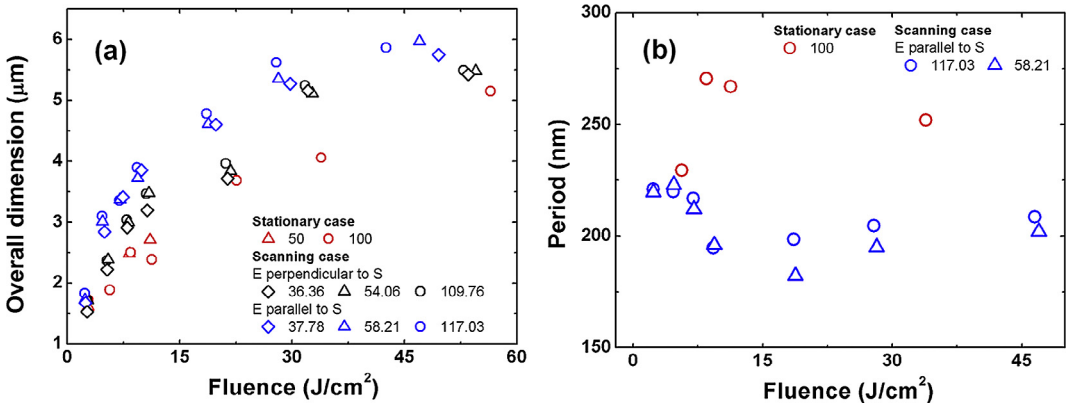

Fig. 8. Comparison of the overall dimensions of modified areas (a) and nanograting periods (b) obtained with certain irradiation parameters in stationary focusing case and dynamic scanning case.

mined by measuring the space between adjacent groove tips along the scan direction. As clearly shown in Fig. 7(f), the period Λs decreases with both of the pulse fluence (for certain scan speed) and scan speed (for fixed pulse fluence), suggesting an enlargement of the angle of grooves with respect to scan direction.

Furthermore, for comparison, the experiment results obtained in stationary case and scanning case that related to similar parameters are shown in Fig. 8, where it is possible to notice that the larger overall dimensions of modified areas could be generated when the incubation factor is greater (as seen from Fig. 8(a)). In the meantime, compared with the stationary case, the spatial frequencies of nanogratings obtained in scanning case are higher when E is parallel to S due to larger incubation factor, as indicated in Fig. 8 (b). Consequently, it can be concluded that the incubation effect plays essential role not only in the process of laser ablation but also in the formation of surface nanogratings on Nd:YAG crystal.

4. Conclusion

In conclusion, comprehensive and parallel studies are performed on the fs-laser induced micro- and nano-sized structures on the surface of Nd:YAG crystal upon irradiation with stationary focusing case and dynamic scanning case. The LIAT fluences and incubation factors of Nd:YAG in both irradiation cases are experimentally determined. In stationary case, the incubation factor of 0.005 is obtained. Meanwhile, the factors are derived to be 0.01 and 0.009, corresponding to two different approaches with E//S and E⊥S in scanning case, respectively. High-spatial-frequency nanogratings with the orientation perpendicular to the beam polarization are produced in the laser ablated regions under both cases. It is indicated that nanogratings of high quality can be fabricated on Nd:YAG surface by properly adjusting the incident laser beam in terms of pulse energy, pulse number or scan speed. In our work, nanograting with period as short as 157 nm is obtained on Nd:YAG surface. This work opens a way to achieve surface nanogratings on Nd:YAG crystal.

Acknowledgements

This work is supported by National Natural Science Foundation of China (No. 11404194), Junta de Castilla y León (Project UIC016), and MINECO (FIS2013-44174-P).

References

[1] R.R. Gattass, E. Mazur, Femtosecond laser micromachining in transparent materials, Nat. Photonics 2 (2008) 219–225.
[2] D.Z. Tan, K.N. Sharafudeen, Y. Yue, J.R. Qiu, Femtosecond laser induced phenomena in transparent solid materials: fundamentals and applications, Prog. Mater. Sci. 76 (2016) 154–228.
[3] C. Phipps, Laser Ablation and Its Applications, Springer, New York, 2006.
[4] S.Z. Xu, J.R. Qiu, T.Q. Jia, C.B. Li, H.Y. Sun, Z.Z. Xu, Femtosecond laser ablation of crystals SiO_2 and YAG, Opt. Commun. 274 (2007) 163–166.
[5] D. Ashkenasi, A. Rosenfeld, H. Varel, M. Wahmer, E.E.B. Campbell, Laser processing of sapphire with picosecond and sub-picosecond pulses, Appl. Surf. Sci. 120 (1997) 65–80.
[6] L. Qi, K. Nishii, M. Yasui, H. Aoki, Y. Namba, Femtosecond laser ablation of sapphire on different crystallographic facet planes by single and multiple laser pulses irradiation, Opt. Lasers Eng. 48 (2010) 1000–1007.
[7] X.X. Li, T.Q. Jia, D.H. Feng, Z.Z. Xu, Ablation induced by femtosecond laser in sapphire, Appl. Surf. Sci. 225 (2004) 339–346.
[8] R.E. Samad, N.D. Vieira Jr., Geometrical method for determining the surface damage threshold for femtosecond laser pulses, Laser Phys. 16 (2006) 336–339.
[9] Y. Shimotsuma, K. Hirao, J. Qiu, K. Miura, Nanofabrication in transparent materials with a femtosecond pulse laser, J. Non-Cryst. Solids. 352 (2006) 646–656.
[10] N. Sanner, O. Utéza, B. Bussiere, G. Coustillier, A. Leray, T. Itina, M. Sentis, Measurement of femtosecond laser-induced damage and ablation thresholds in dielectrics, Appl. Phys. A 94 (2009) 889–897.
[11] J.M. Fernández-Pradas, D. Comas, J.L. Morenza, P. Serra, Irradiation of glass with infrared femtosecond laser pulses, Appl. Phys. A 112 (2013) 203–207.
[12] D. Ashkenasi, M. Lorenz, R. Stoian, A. Rosenfeld, Surface damage threshold and structuring of dielectrics using femtosecond laser pulses: the role of incubation, Appl. Surf. Sci. 150 (1999) 101–106.
[13] F. Liang, R. Vallée, D. Gingras, S.L. Chin, Role of ablation and incubation processes on surface nanograting formation, Opt. Mater. Express 1 (2011) 1244–1250.
[14] H. Lao, H. Zhu, X. Chen, Surface ablation of congruent and Mg-doped lithium niobate by femtosecond laser, Laser Phys. 20 (2010) 245–249.
[15] M. Birnbaum, Semiconductor surface damage produced by ruby lasers, J. Appl. Phys. 36 (1965) 3688–3689.
[16] Y. Shimotsuma, P.G. Kazansky, J. Qiu, K. Hirao, Self-organized nanogratings in glass irradiated by ultrashort light pulses, Phys. Rev. Lett. 91 (2003) 247405.
[17] F. Liang, R. Vallée, S.L. Chin, Mechanism of nanograting formation on the surface of fused silica, Opt. Express 20 (2012) 4389–4396.
[18] M. Rohloff, S.K. Das, S. Höhm, R. Grunwald, A. Rosenfeld, J. Krüger, J. Bonse, Formation of laser-induced periodic surface structures on fused silica upon multiple cross-polarized double-femtosecond-laser-pulse irradiation sequences, J. Appl. Phys. 110 (2011) 014910.
[19] F. Liang, R. Vallée, S.L. Chin, Physical evolution of nanograting inscription on the surface of fused silica, Opt. Mater. 2 (2012) 900–906.
[20] S. Höhm, A. Rosenfeld, J. Krüger, J. Bonse, Femtosecond laser-induced periodic surface structures on silica, J. Appl. Phys. 112 (2012) 014901.
[21] S.K. Das, H. Messaoudi, A. Debroy, E. McGlynn, R. Grunwald, Multiphoton excitation of surface plasmon-polaritons and scaling of nanoripple formation in large bandgap materials, Opt. Mater. Express 3 (2013) 1705–1715.
[22] D. Wortmann, J. Gottmann, N. Brandt, H. Horn-Solle, Micro- and nanostructures inside sapphire by fs-laser irradiation and selective etching, Opt. Express 16 (2008) 1517–1522.
[23] J. Bai, G.H. Cheng, X.W. Long, Y.S. Wang, W. Zhao, G.F. Chen, Polarization behavior of femtosecond laser written optical waveguides in Ti:Sapphire, Opt. Express 20 (2012) 15035–15044.
[24] V.R. Bhardwaj, E. Simova, P.P. Rajeev, C. Hnatovsky, R.S. Taylor, D.M. Rayner, P. B. Corkum, Optically produced arrays of planar nanostructures inside fused silica, Phys. Rev. Lett. 96 (2006) 057404.
[25] W.J. Yang, E. Bricchi, P.G. Kazansky, Self-assembled periodic sub-wavelength structures by femtosecond laser direct writing, Opt. Express 14 (2006) 10117–10124.

[26] S. Richter, M. Heinrich, S. Döring, A. Tünnermann, S. Nolte, Formation of femtosecond laser-induced nanogratings at high repetition rates, Appl. Phys. A 104 (2011) 503–507.
[27] F. Liang, R. Vallée, S.L. Chin, Pulse fluence dependent nanograting inscription on the surface of fused silica, Appl. Phys. Lett. 100 (2012) 251105.
[28] Q. Sun, F. Liang, R. Vallée, S.L. Chin, Nanograting formation on the surface of silica glass by scanning focused femtosecond laser pulses, Opt. Lett. 33 (2008) 2713–2715.
[29] G. Eberle, M. Schmidt, F. Pude, K. Wegener, Laser surface and subsurface modification of sapphire using femtosecond pulses, Appl. Surf. Sci. 378 (2016) 504–512.
[30] R. Wagner, J. Gottmann, Sub-wavelength ripple formation on various materials induced by tightly focused femtosecond laser radiation, J. Phys..: Conf. Ser. 59 (2007) 333–337.
[31] F. Costache, M. Henyk, J. Reif, Modification of dielectric surfaces with ultra-short laser pulses, Appl. Surf. Sci. 186 (2002) 352–357.
[32] D. Dufft, A. Rosenfeld, S.K. Das, R. Grunwald, J. Bonse, Femtosecond laser-induced periodic surface structures revisited: a comparative study on ZnO, J. Appl. Phys. 105 (2009) 034908.
[33] Y. Liu, Y. Brelet, Z.B. He, L.W. Yu, B. Forestier, Y.K. Deng, H.B. Jiang, A. Houardet, Laser-induced periodic annular surface structures on fused silica surface, Appl. Phys. Lett. 102 (2013) 251103.